Check for updates

Aneurysm Inflow-Angle as a Discriminant for Rupture in Sidewall Cerebral Aneurysms

Morphometric and Computational Fluid Dynamic Analysis

Merih I. Baharoglu, MD; Clemens M. Schirmer, MD; Daniel A. Hoit, MD, MPH; Bu-Lang Gao, MD; Adel M. Malek, MD, PhD

Background and Purpose—The ability to discriminate between ruptured and unruptured cerebral aneurysms on a morphological basis may be useful in clinical risk stratification. The objective was to evaluate the importance of inflow-angle (IA), the angle separating parent vessel and aneurysm dome main axes.

Methods—IA, maximal dimension, height–width ratio, and dome–neck aspect ratio were evaluated in sidewall-type aneurysms with respect to rupture status in a cohort of 116 aneurysms in 102 patients. Computational fluid dynamic analysis was performed in an idealized model with variational analysis of the effect of IA on intra-aneurysmal hemodynamics.

Results—Univariate analysis identified IA as significantly more obtuse in the ruptured subset (124.9°±26.5° versus 105.8°±18.5°, $P=0.0001$); similarly, maximal dimension, height–width ratio, and dome–neck aspect ratio were significantly greater in the ruptured subset; multivariate logistic regression identified only IA ($P=0.0158$) and height–width ratio ($P=0.0017$), but not maximal dimension or dome–neck aspect ratio, as independent discriminants of rupture status. Computational fluid dynamic analysis showed increasing IA leading to deeper migration of the flow recirculation zone into the aneurysm with higher peak flow velocities and a greater transmission of kinetic energy into the distal portion of the dome. Increasing IA resulted in higher inflow velocity and greater wall shear stress magnitude and spatial gradients in both the inflow zone and dome.

Conclusions—Inflow-angle is a significant discriminant of rupture status in sidewall-type aneurysms and is associated with higher energy transmission to the dome. These results support inclusion of IA in future prospective aneurysm rupture risk assessment trials. **(*Stroke*. 2010;41:1423-1430.)**

Key Words: angle ■ intracranial aneurysm ■ rupture

Downloaded from http://ahajournals.org by on November 15, 2026

Improvements in vascular imaging methods have led to increased detection of incidental unruptured intracranial aneurysms.[1] In contrast to earlier data, which reported an annual rupture rate of approximately 1% to 2% for unruptured aneurysms,[2,3] recent studies estimate a significantly lower annual rupture risk of 0.1% to 0.2%.[4,5] Although aneurysmal subarachnoid hemorrhage carries a mortality rate of 40% to 50% and a morbidity rate of 10% to 20%,[6,7] preventive surgical or endovascular treatment carries an age-dependent risk of complication. Thus, the decision to treat incidental unruptured aneurysms has to be balanced against the risk of rupture.

Predicting rupture risk for a given incidental aneurysm would be of great clinical value. The quest for such predictors has focused mainly on aneurysm size,[2–5,8,9] location,[4,5,8] and shape.[10–12] Aneurysm aspect ratio (AR)[12] and height–width ratio (H/W)[13] were both found to be higher in ruptured aneurysms. These studies bundled all aneurysm subtypes without segregation between sidewall (SW) and bifurcation-type aneurysms (Figure 1A), a potential confounding factor given computational fluid dynamic (CFD) analysis by Hassan et al[14] suggesting a dichotomy between these subtypes.

CFD analysis of rupture risk has centered on wall shear stress (WSS) and its spatial gradient (WSSG) with studies relating low WSS to aneurysm growth and rupture,[15,16] whereas others find greater WSS[14] and more direct inflow patterns in ruptured aneurysms.[16,17] Greater interest has also been accorded to the morphological relationship between aneurysm and parent vessel because of it influencing intra-aneurysmal flow.[17–20]

The current objective is to evaluate distinguishing morphometric features between ruptured and unruptured SW cerebral aneurysms with special attention to the relationship between parent vessel and aneurysm dome, specifically the inflow-

Received October 18, 2009; final revision received February 12, 2010; accepted March 9, 2010.

From the Cerebrovascular and Endovascular Division, Department of Neurosurgery, Tufts Medical Center and Tufts University School of Medicine, Boston, Mass.

Correspondence to Adel M. Malek, MD, PhD, Department of Neurosurgery, Tufts Medical Center, 800 Washington Street #178, Proger 7, Boston, MA 02111. E-mail amalek@tuftsmedicalcenter.org

© 2010 American Heart Association, Inc.

Stroke **is available at http://stroke.ahajournals.org** **DOI: 10.1161/STROKEAHA.109.570770**

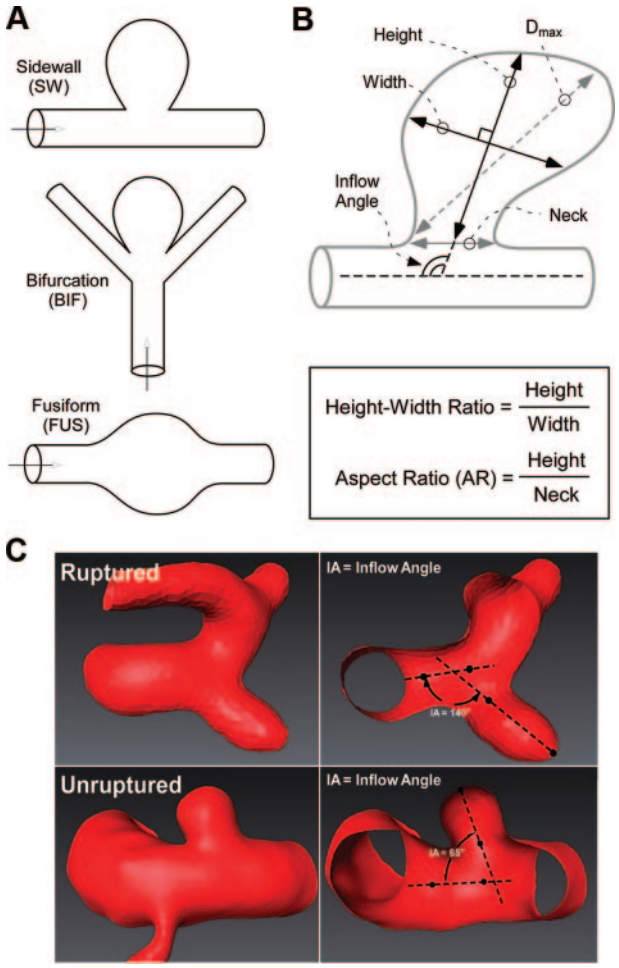


Figure 1. A, Morphological differences in SW, bifurcation-, and fusiform-type aneurysms. B, Schematic of aneurysm dimensions with definition of H/W and AR. B, Illustration of IA measurement in 3-dimensional space in a ruptured (top, IA=140°) and unruptured (bottom, IA=65°) aneurysm.

angle (IA) between flow in the parent vessel and the aneurysm dome axis.

Materials and Methods

Patient Selection and Demographics

All patients with cerebral aneurysms were included in the period spanning September 2001 to April 2009. SW aneurysms were defined as lesions emanating off the side of the parent vessel either without or with a very small vascular branch. A total of 463 aneurysms in 401 patients was selected based on 3-dimensional angiographic availability. After excluding mycotic, peripheral, fusiform, and extradural lesions, based on the latter's different natural history and lower rupture risk,[21] 330 aneurysms remained, of which 116 were SW-type. Clinical information was retrieved from a prospectively maintained database.

Aneurysm Morphology Measurement

Three-dimensional cerebral angiograms were obtained from either Philips Integris (Bothel, Wash) or Siemens Artis (Malvern, Pa) biplane systems and reconstructed using their respective clinical software packages. Volumetric data sets, including aneurysm and parent vessel, were analyzed in Amira Version 4.1 (Mercury Computer Systems, Chelmsford, Mass) to measure in 3-dimensional space (Figure 1B): maximal dome dimension (D_{max}); longest dimension from neck to dome tip (height: H); dome width perpendicular to height (W); and neck width (N). AR was computed by dividing height by neck width[12] and H/W by aneurysm width.[13] IA was measured as the angle between axis of flow in the parent vessel at the level of the aneurysm neck and the aneurysm's main axis from the center of the neck to the tip of the dome (Figure 1C).

Statistical Analysis

JMP Version 5 (SAS Institute, Cary, NC) was used for statistical analysis with significance assumed for $P<0.05$. Characteristics were evaluated independently using Student t test assuming unequal variances and with multivariate logistic regression to analyze interdependence. Receiver operating characteristic curve analysis was used to determine sensitivity and specificity.

Computational Fluid Dynamics

Aneurysm Model and Computational Method

Aneurysm models were constructed with Solidworks (Concord, Mass) measuring 8×4 mm off a 4-mm diameter vessel with IA between 60° and 140° in 10° increments. This parametric design included a spherical neck connector ensuring constant neck and aneurysm dimensions irrespective of IA. The neck was >5 diameters downstream from the inflow, enabling fully developed flow.[22] A second model was constructed on the outer bend of a circular curved geometry with varying IA in plane with parent vessel curvature.[23]

High-resolution polyhedral meshes with prismatic boundary layer enrichment were generated with Star-CCM+ Version 4.02 (CD-Adapco, Melville, NY) at a count of approximately 1 000 000 cells. For comparison and validation of grid size independence,[24] hybrid hexahedral meshes (approximately 450 000 cells) were generated with Harpoon Version 3.4 (Sharc Ltd, Manchester, UK). Finite-volume solution used Fluent Version 6.3.26 (Ansys, Lebanon, NH) in the laminar double-precision unsteady regime,[24] assuming rigid nonslip wall conditions, blood viscosity of 3.5 cP, and density of 1070 kg/m^3. A 1000-timestep pulse was derived from Ford et al[25] with time-average inlet velocity of 0.25 m/s with R_e=371 and Womersley number[22] of 3.3.[23,26]

Postprocessing and Data Analysis

Postprocessing was performed in Ensight Version 9 (CEI, Apex, NC).[24] The net-flow and kinetic energy crossing an orthogonal cut plane halfway toward the dome tip was computed by integrating unidirectional normal velocities and energies. Shear jet zone size was defined as the height from the neck to the 50th percentile of the WSS contour. Velocity jet distance to tip was measured from the 50th percentile velocity contour to the dome tip on a midlongitudinal cut plane.

Results

Demographics and Aneurysm Location

One hundred sixteen SW aneurysms in 102 patients, mean age 56 years (range, 28 to 89 years), were analyzed. Eighty-four patients (82%) were female and 24 aneurysms (21%) had ruptured. Lesion location was 51 paraclinoid internal carotid, 27 posterior communicating, 23 carotid ophthalmic, 7 anterior choroidal, 4 vertebral, 2 posterior cerebral, 1 basilar, and 1 anterior cerebral artery.

Morphological Features

Univariate Statistical Analysis

Aneurysms were divided into ruptured and unruptured subsets. IA was significantly higher for the ruptured group at

Downloaded from http://ahajournals.org by on November 15, 2026

Table. Univariate and Multivariate Analysis of Aneurysm Discriminants*

Morphometric Feature	Ruptured	Unruptured	Univariate *P*	Area Under Receiver Operating Characteristic	Multivariate *P*
Gender	24 (21 female; 3 male)	92 (74 female; 18 male)	0.4	…	…
Age, years	62.8±13.8	54.3±14.5	0.01	…	…
IA, degrees	124.9±26.5	105.8±18.5	0.0001	0.71	0.0158
D_{max}, mm	9.1±3.7	6.2±3.1	0.0002	0.75	0.0705
H/W	1.60±0.71	1.07±0.36	<0.0001	0.76	0.0017
AR	1.88±0.67	1.36±0.64	0.0007	0.73	0.5681

*Shown are means with SD.

124.9°±26.5° compared with 105.8°±18.5° for the unruptured (P=0.0001). D_{max}, H/W, and AR also showed significantly greater values in the ruptured subset (Table; Figure 2A). Receiver operating characteristic analysis showed H/W to have the largest area under the curve (0.76) followed by D_{max} (0.75), AR (0.73), and IA (0.71; Figure 2B).

Multivariate Logistic Regression

The multivariate logistic regression model using D_{max}, IA, H/W, and AR showed only IA (P=0.0158) and H/W (P=0.0017) to be statistically significant morphological discriminants of previous aneurysm rupture (Table). No dependence of IA or H/W on age or gender was observed.

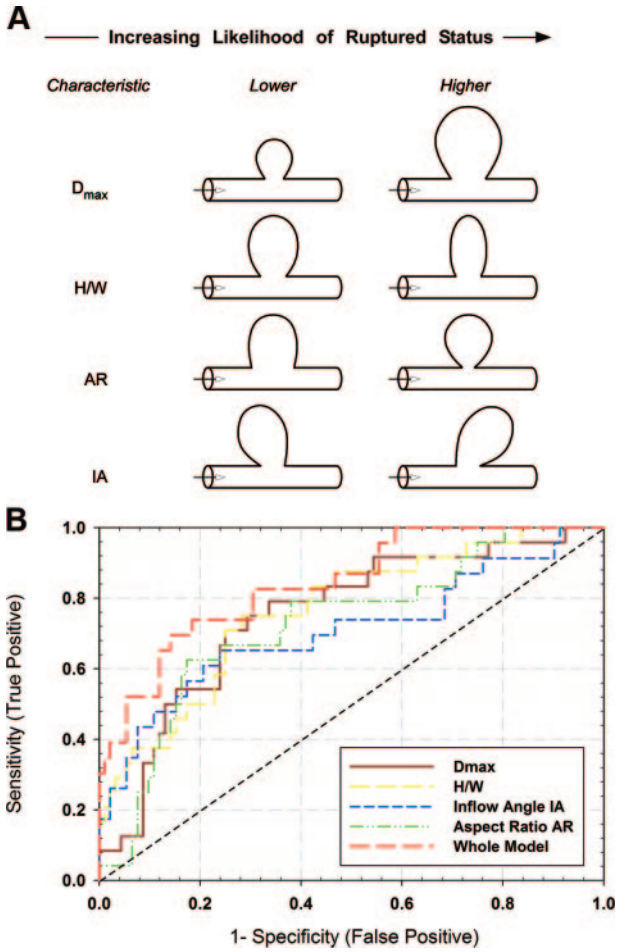


Figure 2. A, Schematic illustrating isolated changes in discriminant characteristic (higher value on right) along with a left-to-right increased likelihood of ruptured status. B, Receiver operating characteristic curves for all discriminants in univariate and for the whole model in multivariate analyses.

Computational Fluid Dynamic Analysis

Inflow Velocity Pattern With Respect to IA

Increasing IA, holding all other parameters and dimensions constant (Figure 3A), led to an increase in the size of the shear jet zone at the base of the aneurysm. This was accompanied by a progressively and comparatively greater and deeper migration of the velocity jet into the dome as measured by distance between jet zone and dome tip (Figure 3B–C).

IA Effect on Net Flow and Kinetic Energy Halfway to the Aneurysm Dome Tip

Analysis of flow parameters through an orthogonal cut plane at 50% from the neck to dome tip revealed significant higher peak flow velocity with higher IA increasing 80-fold from 0.004 m/s at 60° to 0.32 m/s at 140° (Figure 4A–C). Net directional flow traveling across the cut plane increased significantly by 223% (0.0065 mL/s to 0.021 mL/s) from 60° to 120° IA with gentle falloff beyond that point (Figure 4D). In contrast, peak kinetic energy transmission through the cut plane toward the dome tip increased 20-fold from 9.2×10^{-9} J at 60° to 1.8×10^{-7} J at 140° IA (Figure 4E).

Aneurysm Dome WSS Dependence on IA

WSS magnitude measured along a longitudinal cut plane inside the parent vessel and aneurysm dome (Figure 5A) exhibited the expected drop in value within the dome. There was little WSS and WSSG variation at the neck inflow and outflow owing to the design of the model, which kept a constant neck area. Consistent with increasing IA leading to higher flow velocities deeper in the dome, higher IA led to a 7.2-fold WSS increase (6.28×10^{-5} Pa to 4.5×10^{-4} Pa) in the minimum value at the dome with WSSG increasing 5.6-fold (0.014 Pa/m to 0.079 Pa/m; Figure 5B, D). This increase was persistent independent of dynamic phenomena during the cardiac cycle and was observed in both straight and curved parent vessel models (data not shown).

Discussion

IA as a Morphological Discriminant

The current study, based on high-resolution 3-dimensional rotational angiographic data, supplemented by parametric

Downloaded from http://ahajournals.org by on November 15, 2026

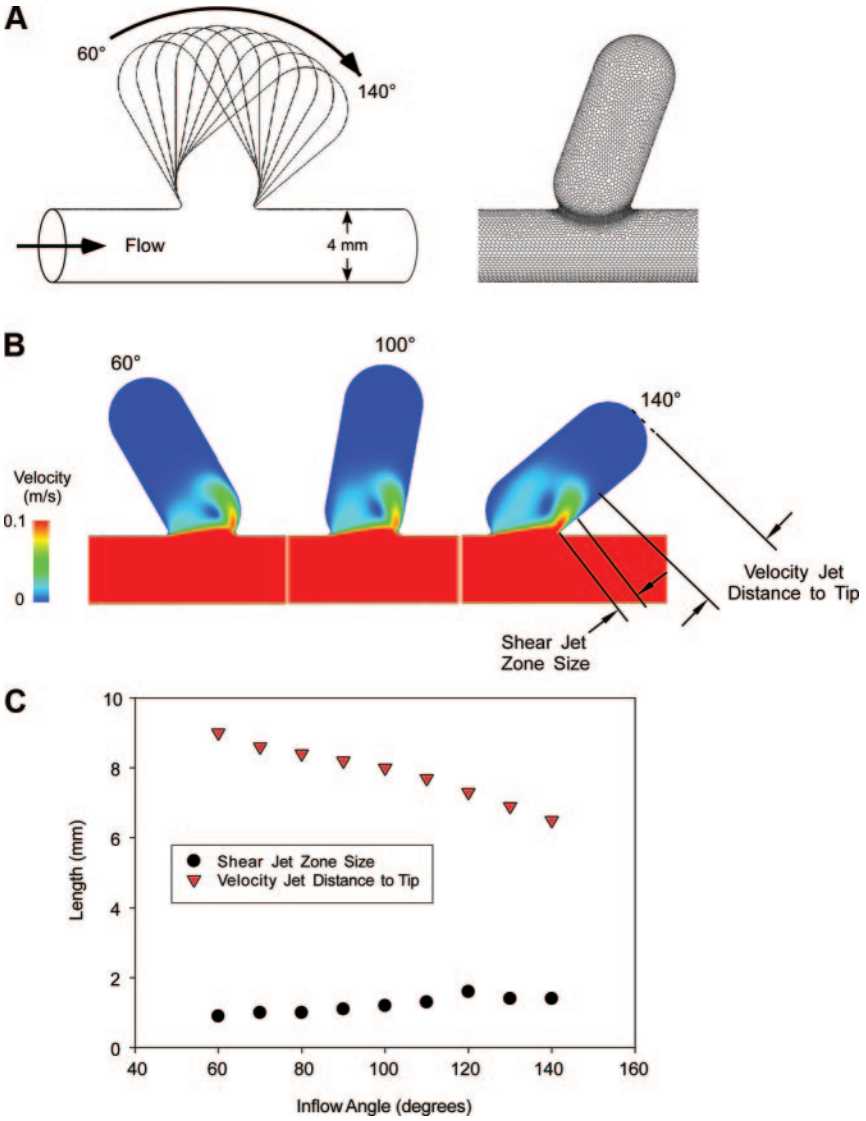


Figure 3. A, Parametric isolated variation of IA from 60° to 140° in 10° increments in a 3-dimensional model based off a 4-mm parent vessel with typical polyhedral surface mesh (right). B, Cross-sectional velocity map inside aneurysm at 60°, 100°, and 140°. C, Increase in size of the shear jet zone and decrease in velocity jet distance to the dome tip with increasing IA.

Downloaded from http://ahajournals.org by on November 15, 2026

CFD modeling, identifies aneurysmal IA as an independent discriminant of rupture status in SW aneurysms, which appears to be statistically more robust than aneurysm size. This finding is consistent with prior descriptive observations by investigators reporting more direct flow into the aneurysm dome[16,18] and more often a parallel axis of the aneurysm relative to the parent vessel[17] in ruptured aneurysms. Although most aneurysm rupture-risk morphological analyses[8,10] such as AR[12] and nonsphericity[10] consider the aneurysm dome as a separate entity detaching it from the neck up, our analysis of IA incorporates the relation of the aneurysm dome to the parent vessel. This spatial relationship has been shown to be an important determinant of flow patterns inside the aneurysm dome[19,23] and may influence rupture risk, consistent with our idealized CFD model findings. A recent study by Dhar et al[27] evaluated the angle of inclination between the aneurysm dome and its neck plane; although significantly different in their ruptured subset, the angle of inclination between the aneurysm dome and its neck plane was not found to be an independent discriminant in a multivariate analysis. This may highlight the greater importance of the relative direction of flow in parent vessel with the dome itself rather than the inflow zone at the neck.

Inflow Jet Velocity and Kinetic Energy

We opted not to use patient-derived angiographic data for CFD modeling, but instead elected to define parametric models allowing us to vary IA independently of the multitude of other morphometric features, at the same time keeping specific variables, including neck size, dome height, and width, constant. This approach enables the independent isolation of the hemodynamic effect of varying IA without including confounding variables such as neck inclination angle, neck surface area, or lateral angle with respect to parent vessel curvature.[23] The constant neck parameters in our model enable us to attribute hemodynamic differences purely to changes in IA. This reductionist approach uncovered important effects with increasing IA, including inward migration of the flow recirculation core into the aneurysm dome and signifi-

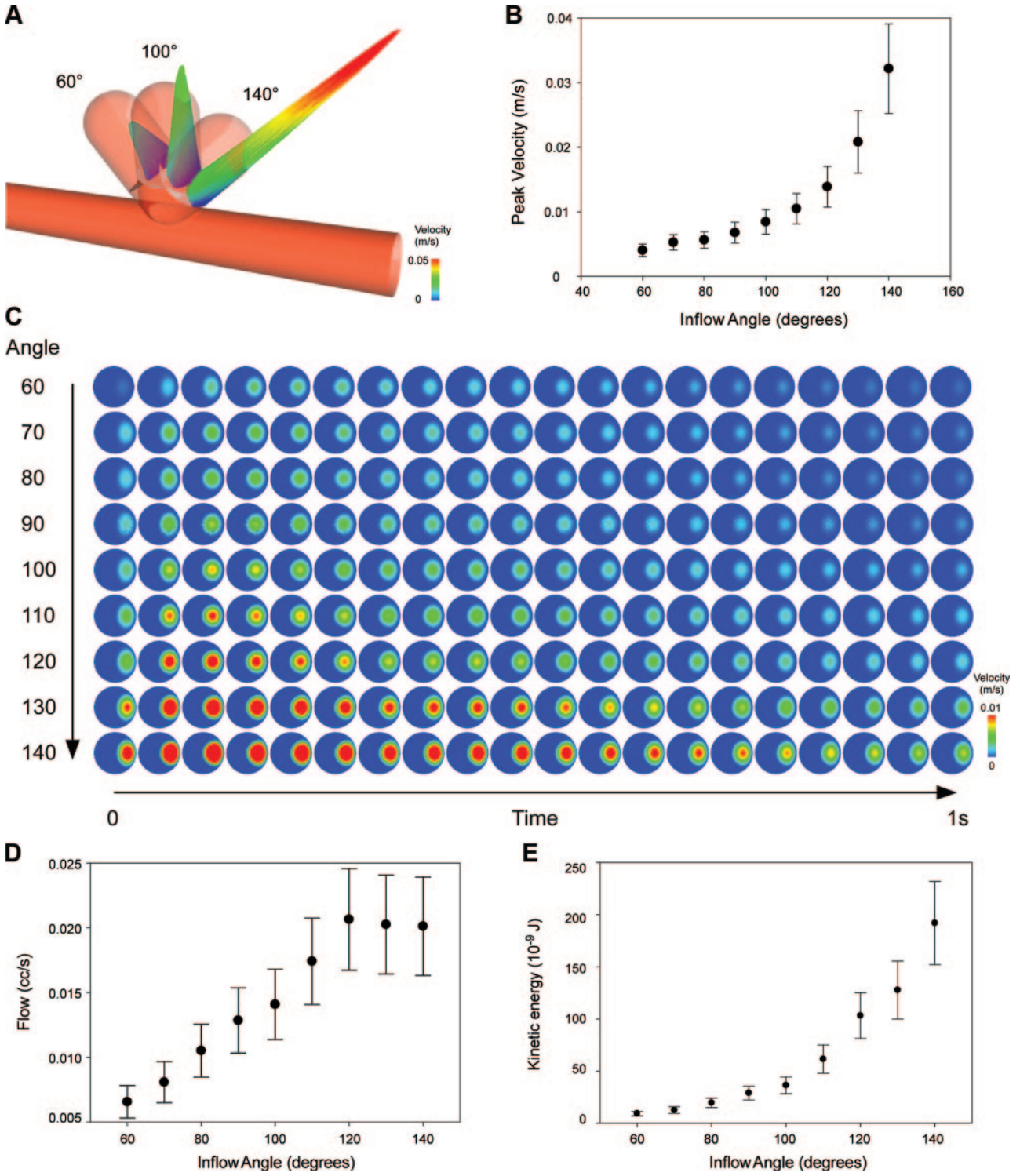


Figure 4. A, Three-dimensional velocity contour of fluid velocity profile in a plane orthogonal to the aneurysm dome main axis at 60°, 100°, and 140°. B, Graph of peak velocity along main axis of aneurysm dome showing a sharp increase with higher IA. C, In-plane velocity color map halfway to the dome tip along 20 time points during pulse cycle with increasing IA. D, Net unidirectional volume flow and kinetic energy (E) at a plane halfway to the dome tip.

cantly higher peak velocities and kinetic energy transmission into the distal dome. Although the current analysis assumes a rigid wall, such increased focal velocity and energy impact is likely to result in greater focal wall tension in a more physiological viscoelastic model of the aneurysm wall, a phenomenon demonstrated recently in a fluid–structure interaction model.[28] Although beyond the scope of the current study, such an approach, especially accounting for nonuniform anisotropic viscoelasticity and aneurysm wall thickness, may be valuable in furthering our understanding of aneurysm rupture despite its high computational demand.

Downloaded from http://ahajournals.org by on November 15, 2026

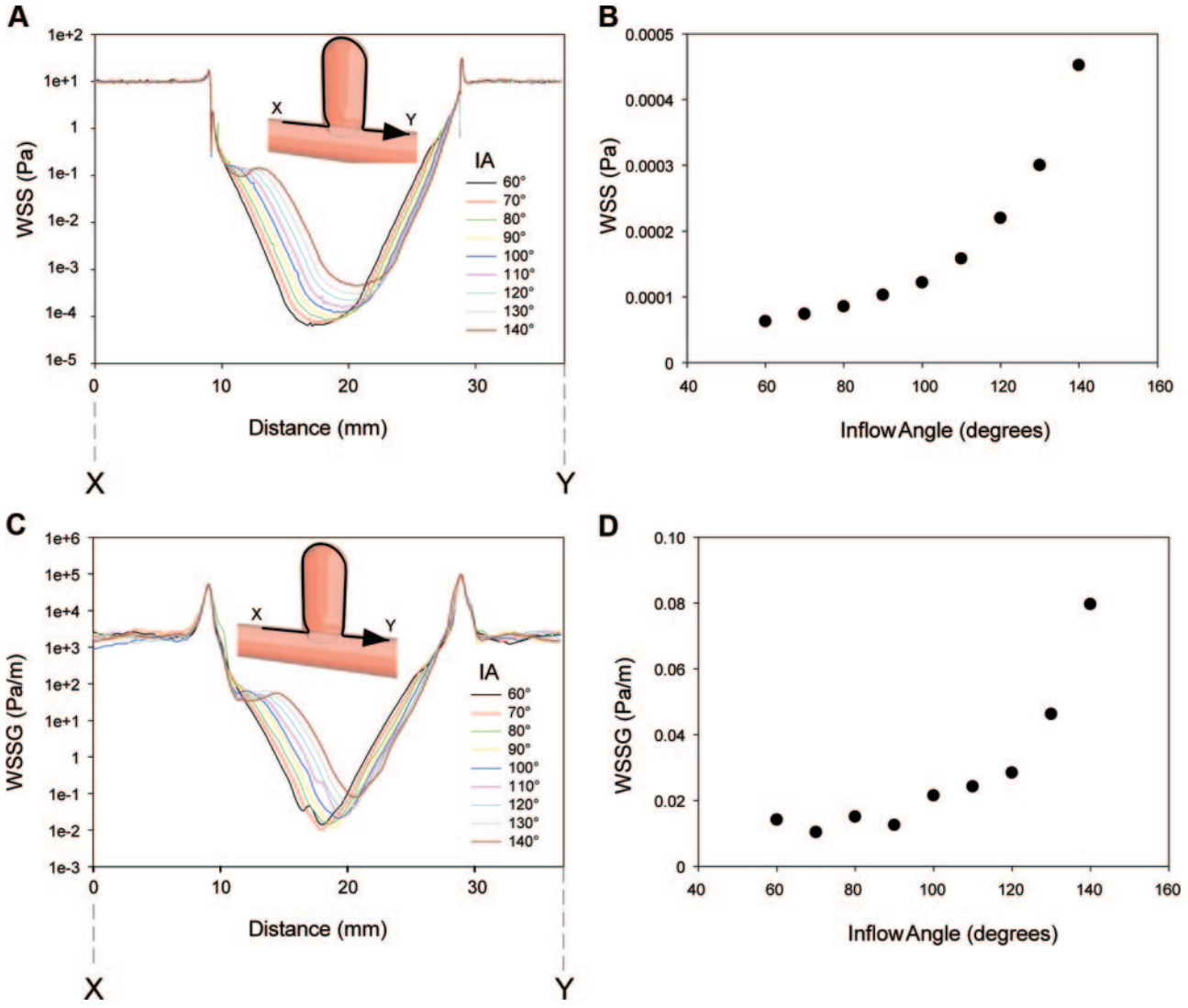


Figure 5. One-dimensional profile of WSS (A–B) and WSSG (C–D) along a midcutline illustrating increasing WSS and WSSG with increasing IA at peak systole.

Downloaded from http://ahajournals.org by on November 15, 2026

WSS and Spatial Gradient

Previous studies[16] have linked low WSS to aneurysm rupture through focal endothelial dysfunction.[29] Other investigations have postulated a higher average WSS in ruptured aneurysms[16] and in rupture areas.[14] Although our data showed higher WSS in the dome of aneurysms with greater IA, these values remain significantly lower than in the parent vessel (by >3 orders of magnitude at the dome tip). The levels of WSS in the majority of the dome for all IA values in this study is lower than 0.1 Pa, a value at which aortic endothelial cells in vitro do not express the flow-sensitive phenotype.[30,31] In fact, flow-mediated endothelin-1 and endothelial nitric oxide synthase shear-induced expression is not activated by shear values <0.4 Pa.[31] High spatiotemporal WSSG are known to induce endothelial cell migration away from the high WSS area[29] both in vitro and in animal models. Meng et al[32] showed that a high product of WSS and WSSG can lead to destructive remodeling of the endothelial layer and subjacent vessel wall; such combination of high WSS and WSSG was found at the neck inflow zone in our model but was largely unaffected by IA variation owing to the design of the model with fixed neck region parameters. Evaluation of the product of WSS and WSSG in the dome of our model aneurysm reveals it to be much too low to be affected by the phenomena described by Tardy[29] and Meng.[32]

Putative Aneurysm Rupture Mechanism

The WSS values at all IA tested for the model used here are very low in the dome; accordingly at the dome tip, both high and low IA models would be characterized by varying but similar degrees of endothelial dysfunction because of the low focal hemodynamic WSS, resulting in the expression of the static deleterious endothelial phenotype.[30,31] In that context, we hypothesize that higher peak velocity and transmitted energy of the flow-jet hitting the dome with increasing IA (increasing by approximately 1 order of magnitude between IAs of 60° and 140°) is likely the driving force behind further tensile strain and deflection of the degenerated focal wall in the region of the dysfunctional endothelium. We pro-

pose that rupture may be the result of 2 pathological mechanisms: first, focal degenerative changes driven by endothelial dysfunction in regions of low WSS[16] (such as blebs and daughter components), and second, coincident elevated wall tension and strain resulting from high velocity and kinetic energy influx on such a degenerative weakened wall region,[32] leading to supramaximal wall deflection and aneurysm rupture.

We limited our analysis to SW aneurysms on a straight segment and on a curved segment model IA in-plane with parent vessel curvature; it is possible that results may differ for other lateral angles as described by Liou et al.[23] In contrast to SW lesions, bifurcation aneurysm hemodynamics are dependent on the relative size and the multiple relative angles of the daughter vessels, introducing significant complexities to the analysis. Paradoxically, in a symmetrical bifurcation, an inline IA of 180° would result in an area of stasis and low flow in the dome, leading to lower velocity, kinetic energy, and WSS compared with a lower IA (data not shown).

Study Limitations

Shape analysis to differentiate between ruptured and unruptured aneurysms assumes that the process of rupture itself does not alter aneurysm shape, a hypothesis that has not yet been conclusively ruled out.

Our data are retrospective in nature and, although we identified a parameter whose importance was further validated by CFD analysis, will need additional prospective testing of their predictive potential.

Our CFD approach assumes rigid walls and does not take into account the viscoelasticity of the vessel wall and the focal anisotropic degenerative changes usually observed in vivo in the aneurysm.

Finally, aneurysm rupture is likely precipitated by several aneurysm characteristics. Mathematical models predicting aneurysm rupture status have been proposed before[8,27] and work on such a model incorporating IA is currently underway and could be further refined by addition of multicenter data.

Conclusion

The current study has identified IA as an independent and robust rupture status differentiator in SW intracranial intradural aneurysms. Although D_{max}, AR, and H/W were separately significantly higher in the ruptured subset, only IA and H/W were independent discriminants and were more important than maximal aneurysm size, the more conventional morphological feature that has been relied on in clinical risk stratification.[5] Future prospective analyses may benefit from inclusion of higher-order shape descriptors and parent vessel–aneurysm relationship analysis such as IA.

Disclosures

None.

References

1. Vernooij MW, Ikram MA, Tanghe HL, Vincent AJ, Hofman A, Krestin GP, Niessen WJ, Breteler MM, van der Lugt A. Incidental findings on brain MRI in the general population. *N Engl J Med*. 2007; 357:1821–1828.
2. Juvela S, Porras M, Poussa K. Natural history of unruptured intracranial aneurysms: probability of and risk factors for aneurysm rupture. *J Neurosurg*. 2000;93:379–387.
3. Yasui N, Magarisawa S, Suzuki A, Nishimura H, Okudera T, Abe T. Subarachnoid hemorrhage caused by previously diagnosed, previously unruptured intracranial aneurysms: a retrospective analysis of 25 cases. *Neurosurgery*. 1996;39:1096–1100; discussion 1100–1191.
4. Unruptured intracranial aneurysms—risk of rupture and risks of surgical intervention. International study of unruptured intracranial aneurysms investigators. *N Engl J Med*. 1998;339:1725–1733.
5. Wiebers DO, Whisnant JP, Huston J III, Meissner I, Brown RD Jr, Piepgras DG, Forbes GS, Thielen K, Nichols D, O'Fallon WM, Peacock J, Jaeger L, Kassell NF, Kongable-Beckman GL, Torner JC. Unruptured intracranial aneurysms: natural history, clinical outcome, and risks of surgical and endovascular treatment. *Lancet*. 2003;362:103–110.
6. Broderick JP, Brott TG, Duldner JE, Tomsick T, Leach A. Initial and recurrent bleeding are the major causes of death following subarachnoid hemorrhage. *Stroke*. 1994;25:1342–1347.
7. Fogelholm R, Hernesniemi J, Vapalahti M. Impact of early surgery on outcome after aneurysmal subarachnoid hemorrhage. A population-based study. *Stroke*. 1993;24:1649–1654.
8. Prestigiacomo CJ, He W, Catrambone J, Chung S, Kasper L, Pasupuleti L, Mittal N. Predicting aneurysm rupture probabilities through the application of a computed tomography angiography-derived binary logistic regression model. *J Neurosurg*. 2009;110:1–6.
9. Wiebers DO, Whisnant JP, O'Fallon WM. The natural history of unruptured intracranial aneurysms. *N Engl J Med*. 1981;304:696–698.
10. Raghavan ML, Ma B, Harbaugh RE. Quantified aneurysm shape and rupture risk. *J Neurosurg*. 2005;102:355–362.
11. Rohde S, Lahmann K, Beck J, Nafe R, Yan B, Raabe A, Berkefeld J. Fourier analysis of intracranial aneurysms: towards an objective and quantitative evaluation of the shape of aneurysms. *Neuroradiology*. 2005; 47:121–126.
12. Ujiie H, Tamano Y, Sasaki K, Hori T. Is the aspect ratio a reliable index for predicting the rupture of a saccular aneurysm? *Neurosurgery*. 2001; 48:495–502; discussion 502–593.
13. Hoh BL, Sistrom CL, Firment CS, Fautheree GL, Velat GJ, Whiting JH, Reavey-Cantwell JF, Lewis SB. Bottleneck factor and height–width ratio: association with ruptured aneurysms in patients with multiple cerebral aneurysms. *Neurosurgery*. 2007;61:716–722; discussion 722–723.
14. Hassan T, Timofeev EV, Saito T, Shimizu H, Ezura M, Matsumoto Y, Takayama K, Tominaga T, Takahashi A. A proposed parent vessel geometry-based categorization of saccular intracranial aneurysms: computational flow dynamics analysis of the risk factors for lesion rupture. *J Neurosurg*. 2005;103:662–680.
15. Boussel L, Rayz V, McCulloch C, Martin A, Acevedo-Bolton G, Lawton M, Higashida R, Smith WS, Young WL, Saloner D. Aneurysm growth occurs at region of low wall shear stress: patient-specific correlation of hemodynamics and growth in a longitudinal study. *Stroke*. 2008;39: 2997–3002.
16. Shojima M, Oshima M, Takagi K, Torii R, Hayakawa M, Katada K, Morita A, Kirino T. Magnitude and role of wall shear stress on cerebral aneurysm: computational fluid dynamic study of 20 middle cerebral artery aneurysms. *Stroke*. 2004;35:2500–2505.
17. Szikora I, Paal G, Ugron A, Nasztanovics F, Marosfoi M, Berentei Z, Kulcsar Z, Lee W, Bojtar I, Nyary I. Impact of aneurysmal geometry on intraaneurysmal flow: a computerized flow simulation study. *Neuroradiology*. 2008; 50:411–421.
18. Cebral JR, Castro MA, Burgess JE, Pergolizzi RS, Sheridan MJ, Putman CM. Characterization of cerebral aneurysms for assessing risk of rupture by using patient-specific computational hemodynamics models. *AJNR Am J Neuroradiol*. 2005;26:2550–2559.
19. Sato K, Imai Y, Ishikawa T, Matsuki N, Yamaguchi T. The importance of parent artery geometry in intra-aneurysmal hemodynamics. *Med Eng Phys*. 2008;30:774–782.
20. Imai Y, Sato K, Ishikawa T, Yamaguchi T. Inflow into saccular cerebral aneurysms at arterial bends. *Ann Biomed Eng*. 2008;36:1489–1495.
21. Kupersmith MJ, Hurst R, Berenstein A, Choi IS, Jafar J, Ransohoff J. The benign course of cavernous carotid artery aneurysms. *J Neurosurg*. 1992; 77:690–693.

Downloaded from http://ahajournals.org by on November 15, 2026

22. Womersley JR. Method for the calculation of velocity, rate of flow and viscous drag in arteries when the pressure gradient is known. *J Physiol*. 1955;127:553–563.
23. Liou TM, Li YC, Juan WC. Numerical and experimental studies on pulsatile flow in aneurysms arising laterally from a curved parent vessel at various angles. *J Biomech*. 2007;40:1268–1275.
24. Schirmer CM, Malek AM. Prediction of complex flow patterns in intracranial atherosclerotic disease using computational fluid dynamics. *Neurosurgery*. 2007;61:842–851; discussion 852.
25. Ford MD, Alperin N, Lee SH, Holdsworth DW, Steinman DA. Characterization of volumetric flow rate waveforms in the normal internal carotid and vertebral arteries. *Physiol Meas*. 2005;26:477–488.
26. Ahmed SA, Giddens DP. Pulsatile poststenotic flow studies with laser Doppler anemometry. *J Biomech*. 1984;17:695–705.
27. Dhar S, Tremmel M, Mocco J, Kim M, Yamamoto J, Siddiqui AH, Hopkins LN, Meng H. Morphology parameters for intracranial aneurysm rupture risk assessment. *Neurosurgery*. 2008;63:185–196; discussion 196–197.
28. Isaksen JG, Bazilevs Y, Kvamsdal T, Zhang Y, Kaspersen JH, Waterloo K, Romner B, Ingebrigtsen T. Determination of wall tension in cerebral artery aneurysms by numerical simulation. *Stroke*. 2008;39:3172–3178.
29. Tardy Y, Resnick N, Nagel T, Gimbrone MA Jr, Dewey CF Jr. Shear stress gradients remodel endothelial monolayers in vitro via a cell proliferation-migration-loss cycle. *Arterioscler Thromb Vasc Biol*. 1997; 17:3102–3106.
30. Dai G, Kaazempur-Mofrad MR, Natarajan S, Zhang Y, Vaughn S, Blackman BR, Kamm RD, Garcia-Cardena G, Gimbrone MA Jr. Distinct endothelial phenotypes evoked by arterial waveforms derived from atherosclerosis-susceptible and -resistant regions of human vasculature. *Proc Natl Acad Sci U S A*. 2004;101:14871–14876.
31. Malek AM, Alper SL, Izumo S. Hemodynamic shear stress and its role in atherosclerosis. *JAMA*. 1999;282:2035–2042.
32. Meng H, Wang Z, Hoi Y, Gao L, Metaxa E, Swartz DD, Kolega J. Complex hemodynamics at the apex of an arterial bifurcation induces vascular remodeling resembling cerebral aneurysm initiation. *Stroke*. 2007;38:1924–1931.

Downloaded from http://ahajournals.org by on November 15, 2026